

Extended Bound state In the Continuum for Ultraheavy Photons in photonic lattice

N. D. Le¹, F. Dubois¹, X. Letartre¹, P. Viktorovitch¹, and H. S. Nguyen^{1*}

¹*Université de Lyon, Institut des Nanotechnologies de Lyon, INL/CNRS,
Ecole Centrale de Lyon, 36 avenue Guy de Collongue, 69130 Ecully, France*

(Dated: November 7, 2021)

Here we report on the dispersion engineering of both real and imaginary parts of photonic resonances in photonic crystal via vertical symmetry breaking. Breaking the vertical mirror symmetry of a photonic crystal slab induces a coupling between two leaky resonances of opposite parities. Such hybridization acts on both the real part (i.e. frequency) and the imaginary part (i.e. radiative loss) of Bloch resonances and offers a tailoring of photonic effective mass and creation of Bound states In the Continuum (BICs). In most configurations, the photonic band of interest exhibits two types of BICs: one at the center of the Brillouin zone and one at oblique angle. The first BIC is a symmetry-protected BIC while the second one is a quasi-BIC induced by vertical symmetry-breaking. The overlap of two BICs in the momentum space engenders a large area of ultra-high quality factor around the Γ point, called extended BIC. All numerical results are nicely reproduced by an intuitive analytical model, combining diffractive and symmetry-breaking couplings. Our results propose an unique scheme to study localized-BIC in photonic lattice: ultraheavy photons with infinite lifetime along a broad range of momentum.

I. INTRODUCTION

Bound states In the Continuum (BICs) were first proposed by von Neumann and Wigner in 1929 [1]. They are peculiar confined states having infinite lifetime despite lying within the continuous spectrum of propagating or leaky states. During decades, the subject was considered simply as a mathematical curiosity. It was not until 1977 that Herrick and Stillinger suggested to realize BICs in semiconductor heterostructure superlattices [2, 3]. In 1985, Friedrich and Wintgen explained the origin of BIC by destructive interference of leaky modes radiating into the same radiation channels [4]. This seminal work has led to the study of BICs in various contexts [5]: quantum mechanics [6], water wave [7, 8], solid state physics [9–13], atomic and molecular physics [14–16] and photonics [17–24], both theoretically and experimentally.

Over the last few years, BICs have become an active research topic in the field of nanophotonics. The early works on photonic BICs reported on the existence of symmetry protected BICs at the centre of the Brillouin zone (i.e. Γ -point) in the momentum space of photonic crystal (PC) [18]. These are anti-symmetric modes of in-plane symmetry and cannot couple to plane-waves of the continuum. Out of Γ -point, when the in-plane symmetry is broken, BICs can still be achieved thanks to accidental symmetry obtained via parameter tuning [19, 20]. These fundamental features have led to various applications of BIC in sensing [25], lasing [23, 26] and zero-refractive index material. Remarkably, BICs in photonic lattice were also demonstrated to have topological nature, manifesting in topological charges associated to polarization vortex in the momentum space [5, 21]. Moreover, it was shown recently that the lattice scheme is not strictly necessary for photonic BICs; and quasi-BICs can be obtained

via parameter tuning of a single resonant element such as Mie resonator [27].

In a previous work, we have demonstrated the possibility to engineer on-demand the energy-momentum dispersion of non-radiating photonic bands below the light-line in PC via vertical symmetry breaking [28]. Very recently, we have shown that vertical symmetry breaking also leads to the creation of a new type of off- Γ quasi-BIC in PC, called symmetry-breaking BIC. This is obtained via destructive interference between radiating photonic modes of opposite symmetries [29]. These two works suggest the possibility of dispersion engineering of both real and imaginary component of photonic modes in photonic crystal exhibiting vertical symmetry.

Here we report on the dispersion engineering of Bloch resonances in the complex plane by breaking the vertical mirror symmetry of a PC slab. The hybridization of leaky modes of opposite parities acts on both the real part (i.e. frequency) and the imaginary part (i.e. radiative loss) and offers a tailoring of photonic effective mass and creation of Bound states In the Continuum (BICs). The dispersion shape and location of BICs are freely tuned by simply modifying the filling factor of the PC. In most configurations, the photonic band of interest exhibits two types of BICs: one at the center of the Brillouin zone and one at oblique angle. The first BIC is a symmetry-protected BIC while the second one is a quasi-BIC induced by vertical symmetry-breaking. The overlap of two BICs in the momentum space engenders a large area of ultra-high quality factor around the Γ point, called extended BIC. The numerical results are nicely reproduced by an intuitive analytical model, combining diffractive and symmetry-breaking couplings. Our results propose an unique scheme to study localized-BIC in photonic lattice: ultraheavy photons with infinite lifetime along a broad range of momentum.

* hai-son.nguyen@ec-lyon.fr

II. PRINCIPLE OF DISPERSION ENGINEERING IN THE COMPLEX PLANE VIA VERTICAL SYMMETRY BREAKING

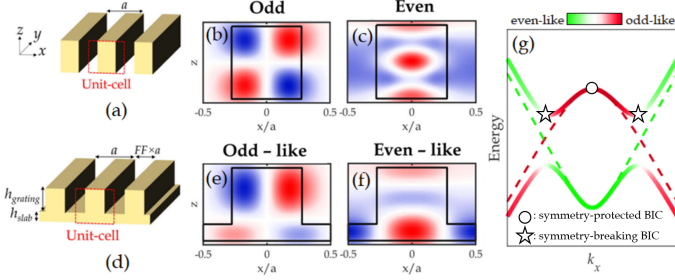


FIG. 1. (a) Sketch of 1D photonic crystal slab having vertical symmetry. The dash rectangle corresponds to a unit cell. (b, c) Distribution of the electric field $E_y(x, y = 0, z)$ of the (b) odd and (c) even mode of the TE-polarization in the structure (a). (d) Sketch of 1D photonic crystal slab with broken vertical symmetry. (e, f) Distribution of the electric field $E_y(x, y = 0, z)$ of the (e) odd-like and (f) even-like mode of the TE-polarization in the structure (d). (g) The coupling between odd-like and even-like modes resulting in multivalley dispersion.

In this section, we discuss on the principle of engineering the real and imaginary parts of Bloch resonances via vertical symmetry breaking. In particular, main ingredients of tailoring the dispersion shape and creating symmetry-breaking BICs will be explained. For the sake of simplicity, this work limits in the case of TE-polarized modes in 1D photonic crystal slab of refractive index $n_{PC} = 3.15$, but our concept can be applied for both 1D and 2D slabs.

We first consider a 1D PC slab having vertical symmetry (i.e. mirror symmetry of symmetry plane $z = 0$) [Fig.1(a)]. Such lattice also has an in-plane symmetry (i.e. mirror symmetry of symmetry plane $x = 0$). TE-polarized Bloch resonances in this structure can be divided into 4 groups of different parities with respect to the two symmetries. To distinguish the in-plane parities to the vertical parities, the terms symmetric and antisymmetric will be used for the in-plane parities; and even and odd for the vertical parities. Bloch resonances can be divided into two groups of opposite parities (i.e. odd and even) with respect to the vertical symmetry. Among different resonances, sorted from lowest to highest energy, we pay a particular attention to two modes: the first odd mode and the second even mode. The electric fields of these modes (i.e. E_y), excited at normal incidence, are presented respectively in Fig.1.(b) and (c). From these field distributions, it is shown that these odd/even modes of vertical symmetry are respectively antisymmetric/symmetric of in-plane symmetry. As consequence, the odd mode is a symmetry-protected BIC at Γ point while the even mode is always leaky mode.

The vertical symmetry of the initial design can be

broken by implementing a residual slab on beneath of the corrugated grating to create ‘comb’ structure [see Fig.1(d)]. Once the vertical symmetry broken, the previous odd and even modes become odd-like [Fig.1(e)] and even-like [Fig.1(f)] modes. On the other hand, the ‘comb’ structure still exhibits in-plane symmetry, thus the odd-like mode remains a symmetry-protected BIC at Γ point and the even-like mode remains a leaky mode. This is confirmed by the antisymmetric/symmetric field distribution of the odd-like/even-like mode and symmetric as shown in Fig.1(e)/(f). However, out of the Γ point, the in-plane symmetry is also broken. Thus it is possible to couple the odd-like to the even-like mode at oblique angle. Noting that the two uncoupled modes have parabolic dispersions of opposite curvature, their coupling will result in a W-shaped and a M-shaped multivalley band [Fig.1(g)]. This is reported in our previous work [28]. Moreover, coupling between radiating modes leads to a creation of quasi-BIC in the vicinity of the anticrossing points [29]. Once the Friedrich-Wintgen condition is satisfied, the destructive interference causes this BIC to become a symmetry-breaking BIC [29]. We choose the design so that this BIC is located on the W-shaped band [Fig.1(g)]. Due to the coexistence of both BICs on the same band, the Q factor becomes high on the dispersion segment bounded by them. This situation is called an extended BIC. The hybridization between odd-like and even-like modes can be finely tuned by modifying the filling factor FF of the design, leading to an engineering of the dispersion diagram and the position of the symmetry-breaking BIC in the momentum space.

III. NUMERICAL RESULTS

In order to demonstrate numerically the extended BIC on ultraflat band, we employ a 1D photonic crystal slab ‘comb’ structure with refractive index $n_{PC} = 3.15$, period $a = 330$ nm, the total height of the comb is 350 nm, consisting of a grating of height $h_{grating} = 270$ nm and a slab with thickness $h_{slab} = 80$ nm. Both the dispersion and the radiative loss were tuned by varying the filling factor FF from 0.60 back to 0.40.

Fig.2 shows the reflectivity spectra of the structures for different values of the filling factor FF , decreasing from 0.55 down to 0.45. The spectra were calculated using the Rigorous Coupled Wave Analysis (RCWA) method [30]. As shown in Fig.2(a), there exist 3 bands, named respectively in order of increasing energy as: Band 1, Band 2, and Band 3. Band 1 has parabola-shaped and negative curvature. At $k_x = 0$, the photonic mode cannot couple with propagating wave, and becomes a symmetry-protected BIC. This is shown in the spectra as the Fano resonance of the band vanishes at $k_x = 0$. Band 2 has multivalley M-shape, is bright, and of large linewidth. The dispersion curve of Band 3 is very thin, so we cannot observe a large portion of the band containing the center of the Brillouin zone in Fig.2(a). Hence, the infor-

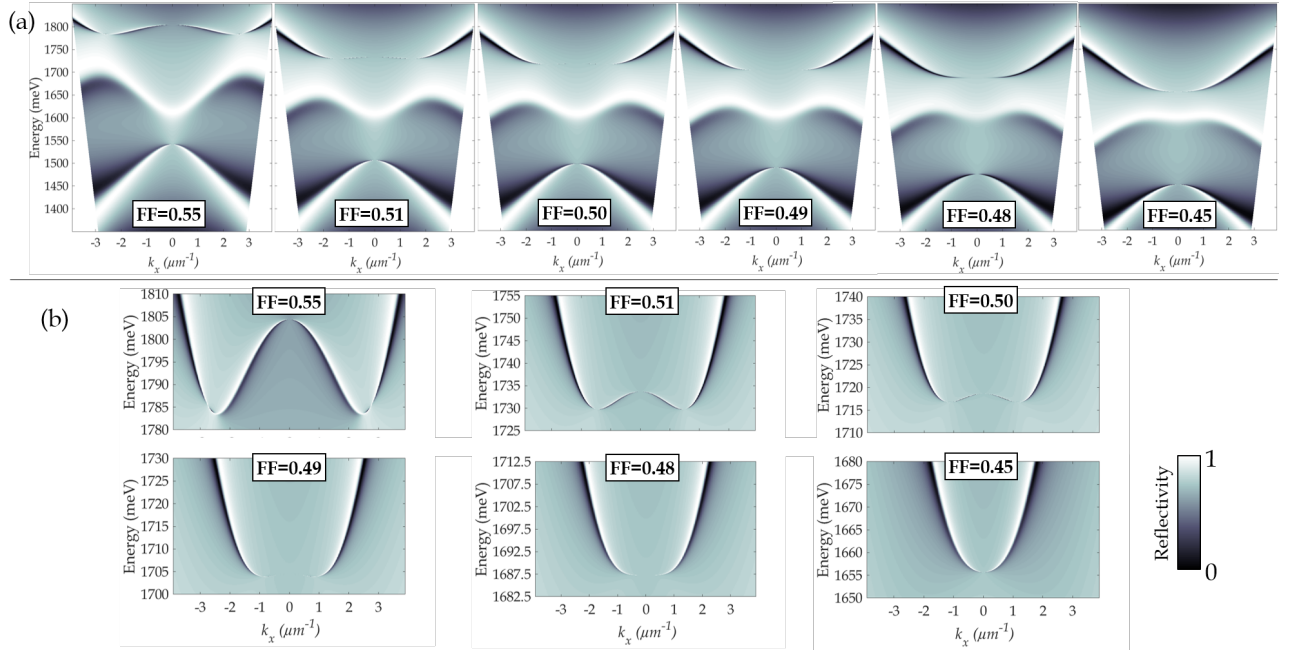


FIG. 2. (a) Reflectivity spectra of the 'comb' structure for different values of the filling factor FF simulated by the RCWA method. (b) Zoom of the reflectivity spectra for the band of highest energy level in (a).

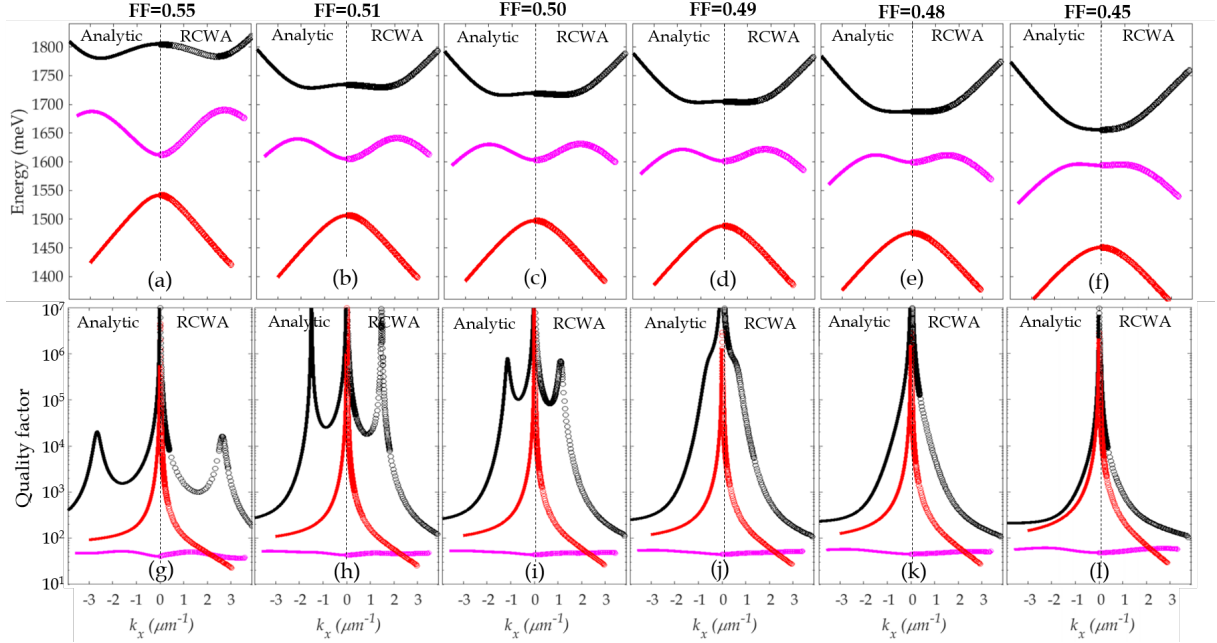


FIG. 3. The dispersion relation (a-f) and the Q factor (g-l) of Band 1 (red), Band 2 (magenta), and Band 3 (black). $k > 0$: results computed by RCWA method. $k < 0$: results calculated by the analytical model.

mation about this band should be given in the zoomed spectra in Fig.2(b). For $FF = 0.55, 0.51, 0.50$, the dispersion curve has multivalley W-shape, with the Fano resonance vanishes at the center of the Brillouin zone. Here we have the second symmetry-protected BIC lo-

cated on Band 3. The dispersion segment between the two anticrossing points becomes thinner as FF decreases, and the Fano resonance almost vanishes in the vicinity of the anticrossing points for $FF = 0.50$ and $FF = 0.51$. For $FF = 0.49$ and $FF = 0.48$, the dispersion segment

around the center of the Brillouin zone still cannot be observed. At $FF = 0.45$, the band has a parabolic dispersion, with a symmetry-protected BIC at $k_x = 0$, similarly to Band 1, but of positive curvature.

As previously shown, we cannot observe the dispersion relation of Band 3 by observing the reflectivity spectra. However, we can consider the resonant modes as forced oscillators excited by incident light, and remark that the absorption satisfies a Lorentzian relation in function of the frequency as demonstrated in Ref. [31]. Hence, from the RCWA calculations for the absorption, we can find the resonant frequencies ω_0 and the linewidth γ of all the 3 bands, and deduce the Q factor of the modes from the formula $Q = \omega_0/\gamma$ as reported in Ref. [5].

The results extracted from the Lorentzian model gave the dispersion relation as shown in Fig.3(a)-(f). The parabolic dispersion of Band 1 and the multivalley dispersion of Band 2 were perfectly reproduced. For Band 1, at $k_x = 0$, the Q factor tends to infinite, confirming the existence of a symmetry-protected BIC. Band 2 has the lowest Q factor, explaining its largest bandwidth comparing to the other two bands. From $FF = 0.55$ to $FF = 0.49$, Band 3 has multivalley dispersion, but becomes flattened as FF increases [see Fig.3(a)-(d)]. At $FF = 0.48$, the band becomes flat [see Fig.3(e)]. By further decreasing FF , we have a parabolic band at $FF = 0.45$ [see Fig.3(f)]. At $k_x = 0$, the Q factor on Band 3 tends to infinite, confirming the existence of the second symmetry-protected BIC as discussed above. At $FF = 0.55$, the Q factor is high ($Q > 10^4$) but finite in the vicinity of the anticrossing point [see Fig.3(g)]. This situation corresponds to a quasi-BIC coexisting with the symmetry-protected BIC on the same band. For $FF = 0.51$, the quasi-BIC accidentally becomes a BIC with infinite Q factor as shown in Fig.3(h). We obtain a second BIC on the band, but not at a symmetry-protected position. Though, at $FF = 0.50$, the BIC becomes again a quasi-BIC [Fig.3(i)]. Note that when decreasing FF , the quasi-BIC approaches the symmetry-protected BIC at the center of the Brillouin zone, leading to a rise in the Q factor in the dispersion segment of the band bounded by them. That explain why this dispersion segment becomes thinner with decreasing FF . At $FF = 0.49$, the quasi-BIC is close enough to the symmetry-protected BIC so the Q factor in this segment becomes as high as at the quasi-BIC ($Q = 10^6$) [see Fig.3(j)], and the dispersion segment becomes thin enough not to be observed in the reflectivity spectra [Fig.2]. By further reducing the filling factor FF to $FF = 0.48$, we obtained an ultraflatband with high Q factor ($Q > 10^5$), and infinite mass photon [see Fig.3(e) and (k)]. When continuing to reduce FF , the dispersion changes to parabola ($FF = 0.45$), with positive curvature, having a symmetry-protected BIC [Fig.3(f) and (l)].

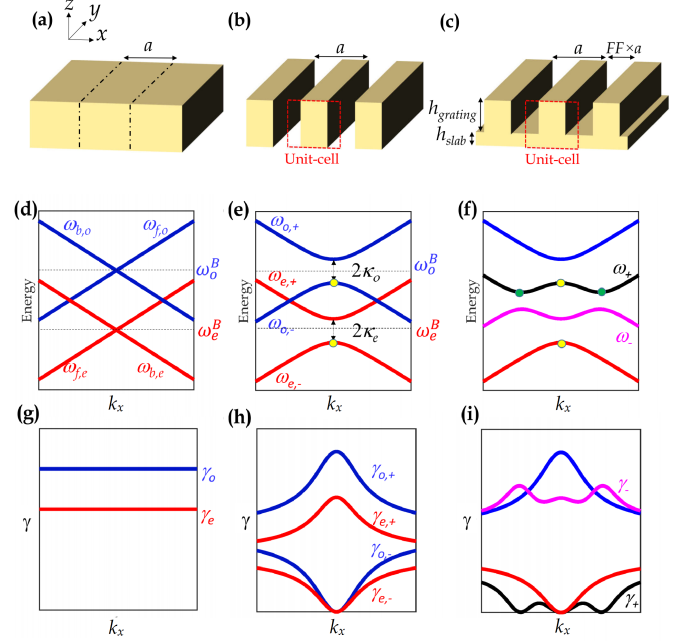


FIG. 4. Line 1: (a) Homogeneous dielectric slab waveguide. (b) 1D photonic crystal with vertical symmetry. (c) 1D photonic crystal with broken vertical symmetry. Line 2: Dispersion curves of: (d) Uncoupled modes in structure (a). (e) Coupled modes in structure (b) due to diffractive coupling. (f) Coupled modes in structure (c) due to symmetry-breaking coupling. Line 3: Radiative loss of: (g) Uncoupled modes in (a). (h) Coupled modes in (b) due to diffractive coupling. (i) Coupled modes in (c) due to symmetry-breaking coupling.

IV. TWO-STEPS COUPLING ANALYTICAL MODEL

To explain the coexistence of the symmetry-protected BIC and the quasi-BIC on the same band, we propose an analytical model based on the coupled-mode theory. We start by considering the forward and backward waves of both the odd and even modes propagating inside a homogeneous dielectric slab waveguide with an effective refractive index [Fig.4(a)]. All these 4 waves have a linear dispersion relation and constant lossy rates as shown in Fig.4(d) and (g):

$$\omega_{f,e(o)}(k_x) = \omega_{e(o)}^B + vk_x \quad (1)$$

$$\omega_{b,e(o)}(k_x) = \omega_{e(o)}^B - vk_x \quad (2)$$

$$\Omega_{f,e(o)}(k_x) = \omega_{f,o(e)}(k_x) - i\gamma_{e(o)} \quad (3)$$

$$\Omega_{b,e(o)}(k_x) = \omega_{b,o(e)}(k_x) - i\gamma_{e(o)} \quad (4)$$

where $\Omega_{f(b),e(o)}$ is the complex resonant frequency of the forward (backward) wave of the even (odd) mode, $\omega_{e(o)}^B$

is the value of the resonant frequency of the wave at $k_x = 0$, v is the group velocity of the waves. The real part $\omega_{f(b),e(o)}(k_x)$ represents the dispersion relation and the imaginary part $\gamma_{e(o)}$ represents the radiative loss of the even (odd) modes.

For a photonic crystal having vertical symmetry as shown in Fig.4(b), the diffractive coupling happens between modes having same parity. The resulting modes conserve the parity of the uncoupled modes. The coupling between even (odd) propagating waves can be solved by finding the eigenvalues of the following Hamiltonians, established by using the coupled-mode theory [32]:

$$H_{e(o)} = \begin{bmatrix} \omega_{e(o),f} & \kappa_{e(o)} \\ \kappa_{e(o)} & \omega_{e(o),b} \end{bmatrix} - i \begin{bmatrix} \gamma_{e(o)} & \gamma_{e(o)} \\ \gamma_{e(o)} & \gamma_{e(o)} \end{bmatrix} \quad (5)$$

where $\kappa_{e(o)}$ represents the diffractive coupling strength of the even (odd) modes. The off-diagonal entries in the imaginary part of the Hamiltonians represent the loss exchange via the radiative channels. The resulting modes $\Omega_{e(o),\pm}(k_x)$ are eigenvalues of these Hamiltonians:

$$\Omega_{e(o),\pm}(k_x) = \omega_{e(o)}^B - i\gamma_{e(o)} \pm \sqrt{(\kappa_{e(o)} - i\gamma_{e(o)})^2 + v^2 k_x^2} \quad (6)$$

The dispersion relation of the resulting modes is represented by:

$$\omega_{e(o),\pm}(k_x) = \text{Re}(\Omega_{e(o),\pm}(k_x)) \quad (7)$$

and the radiative losses of those modes are:

$$\gamma_{e(o),\pm}(k_x) = -\text{Im}(\Omega_{e(o),\pm}(k_x)) \quad (8)$$

Their values as function of k_x are shown in Fig.4(e) and h, respectively. At $k_x = 0$, the real and imaginary parts of the 4 modes are:

$$\omega_{e(o),\pm} = \omega_{e(o)}^B \pm \kappa_{e(o)} \quad (9)$$

$$\gamma_{e(o),+} = 2\gamma_{e(o)} \quad (10)$$

$$\gamma_{e(o),-} = 0 \quad (11)$$

As a result, the bandgap is opened by $2\kappa_{e(o)}$ at $k_x = 0$. Each bandgap is associated to two modes having the same parity but whose dispersion curves have opposite curvature. Moreover, the upper modes gain all the radiative loss, while the lower modes have no radiative loss, and become Bound states In the Continuum (BIC). In other words, the lower modes $\Omega_{e(o),-}$ are antisymmetric, while the upper modes $\Omega_{e(o),+}$ are symmetric. Such BICs, which occur at the high symmetry position in the k -space, are classified as symmetry-protected BICs. By contrast, due to the parity conservation, the modes $\Omega_{e,\pm}$ and $\Omega_{o,\pm}$ have the same parity as the uncoupled modes from which they arise, in terms of vertical symmetry (along the z -direction).

When the symmetry is not broken, even and odd modes are in opposite phase and cannot couple one to the

other. By breaking the vertical symmetry, they are no longer perfectly even and odd modes, but become even-like and odd-like, and are now able to couple between them. Such coupling requires a 4×4 Hamiltonian, thus complicated to be solved analytically. In order to simplify the calculation, we assume that breaking the vertical symmetry implements a perturbation on the modes of the design having vertical symmetry. According to that assumption, the coupling strengths of diffractive couplings are much stronger than the ones in odd-even coupling. Hence, we can first consider the diffractive coupling between modes having the same parity, and later, consider the coupling between modes of opposite parities.

In this perturbation approach, the odd-even coupling is only efficient in the vicinity of the anticrossing points of the band dispersion. Hence, from Fig.4e, we can only consider such coupling between two modes: $\Omega_{o,-}$ and $\Omega_{e,+}$. According to the previous discussion, at $k_x = 0$, those modes have completely opposite parities, so cannot couple one to the other. Hence, the odd-even coupling strength U should depends on k_x and vanishes at $k_x = 0$. Therefore, using $k.p$ method, we can approximate this coupling strength as a linear function of k_x as follows:

$$U = \alpha k_x \quad (12)$$

where α is a constant.

Let $\omega_e = \omega_{e,+}(k_x)$, $\omega_o = \omega_{o,-}(k_x)$, $\Gamma_e = \gamma_{e,+}(k_x)$, and $\Gamma_o = \gamma_{o,-}(k_x)$, we consider the coupling between two modes $\Omega_{e,+}$ and $\Omega_{o,-}$ by solving for the eigenvalues of the following Hamiltonian [33]:

$$H_{comb} = \begin{bmatrix} \omega_e & U \\ U & \omega_o \end{bmatrix} - i \begin{bmatrix} \Gamma_e & \sqrt{\Gamma_e \Gamma_o} e^{i\phi} \\ \sqrt{\Gamma_e \Gamma_o} e^{i\phi} & \Gamma_o \end{bmatrix} \quad (13)$$

Here ϕ is the dephasing between the two modes into the radiative channel. Similar to the diffractive coupling between forward and backward waves, the off-diagonal terms of the imaginary part of the Hamiltonian represent the loss exchange via the radiative channels. The dispersion $\omega_{\pm}(k_x)$ and radiative loss $\gamma_{\pm}(k_x)$ of the corresponding eigenvalues $\Omega_{\pm}(k_x)$ are shown in Fig.4(f) and (i).

$$\Omega_{\pm} = \frac{\omega_o + \omega_e}{2} - i \frac{\Gamma_o + \Gamma_e}{2} \pm \frac{1}{2} \sqrt{[(\omega_o - \omega_e) - i(\gamma_o - \gamma_e)]^2 + 4(U - i\sqrt{\Gamma_o \Gamma_e} e^{i\phi})^2} \quad (14)$$

$$\omega_+ = \text{Re}(\Omega_+) = \omega_o^B - \kappa_o \quad (15)$$

$$\omega_- = \text{Re}(\Omega_-) = \omega_e^B + \kappa_e \quad (16)$$

$$\gamma_+ = -\text{Im}(\Omega_+) = 0 \quad (17)$$

$$\gamma_- = -\text{Im}(\Omega_-) = 2\gamma_e \quad (18)$$

At $k_x = 0$ where the coupling vanishes, the frequencies and radiative losses of the resulting modes remain the same as the modes previously obtained by diffractive coupling. That means, there exists a symmetry-protected BIC on band Ω_+ , inherited from the odd band $\Omega_{o,-}$ of the design having vertical symmetry. Since the two modes $\Omega_{e,-}$ and $\Omega_{o,+}$ are not affected by symmetry-breaking coupling, their dispersions and radiative losses remain unchanged. Overall, we have 4 bands of increasing energy level as shown in Fig.4(f). We remark that the 3 bands: $\Omega_{e,-}$, Ω_- , and Ω_+ correspond to Band 1, Band 2, and Band 3 as previously shown in Fig.2 and Fig.3, respectively. Moreover, there exist two positions in the k -space with opposite k -vector, at which the radiative loss of Band 3 nearly vanishes. They correspond to the quasi- and off- Γ BICs previously discussed in Fig.2 and Fig.3.

This analytical model was used to fit the numerical calculations by fixing $v = 0.253c$ (c is the speed of light in vacuum), the parameters ω_o , γ_o , κ_o , α , and ϕ . The results are shown in Fig.3. The analytic model reproduced perfectly the dispersion relation of the bands, compared to the results extracted from the RCWA calculations of the reflectivity spectra. Concerning the Q factor, it also gave the same position of the BICs and quasi-BICs as the RCWA calculations, and reproduced perfectly the Q factor of Band 2. However, there exists difference in the Q factor calculated by both methods for k_x far away from the BICs and quasi-BICs.

V. PHOTONIC EFFECTIVE MASS AND EXTENSION OF THE BIC

Fig.5(a) shows the ratio m_e/m^* between the rest mass m_e of electron and the effective mass of photons at the position of the two Γ -BICs on Band 1 (red) and Band 3 (black), in function of the filling factor FF . The effective mass m^* of the photon was calculated from the dispersion $E(k_x)$ extracted from the RCWA simulation by the formula [34]:

$$\frac{1}{m^*} = \frac{1}{\hbar^2} \frac{d^2 E}{dk_x^2} \quad (19)$$

By changing the filling factor FF , the ratio m_e/m^* of photon in Band 3 changes from positive ($FF = 0.40 - 0.47$), through 0 ($FF = 0.48$), to negative ($FF = 0.49 - 0.60$). That means, when increasing the filling factor FF , the effective mass of the photon at Γ -point of Band 3 varies from positive (parabolic dispersion), to infinite (ultraflat band), and becomes finally negative (multivalley dispersion). When FF differs from the value at which there exists an ultraflat band, the effective

mass of photon decreases in absolute value, that means the photon becomes lighter. Similarly, the ratio m_e/m^* decreases monotonically in function of FF for the photon at the Γ -point of Band 1, the effective mass of the photon remains negative and decreases in absolute value when FF increases. In other words, the photon becomes lighter and lighter as FF increases. Although the photon in Band 1 is heavier than the photon in Band 3 at $FF = 0.40$ ($m_e/m^* = -4 \times 10^5$ for Band 1 against 6×10^5 for Band 3), as FF increases, the former becomes lighter and lighter while the later becomes heavier and infinitely massive in the case where we have a flatband. When Band 3 changes from ultraflat band to multivalley dispersion, the photon at Γ -point becomes lighter and lighter as FF increases, with negative effective mass. However, the photon at Γ -point of Band 3 is already much lighter than the one in Band 1, and its effective mass reduces much faster. At $FF = 0.60$, $m_e/m^* = -2 \times 10^5$ for Band 3, but -14×10^5 for Band 1. That means, the photon at Γ -point of Band 1 is 7 times lighter than the photon at Γ -point of Band 3.

To estimate how massive is a photon on these two bands, we compare the effective mass of photon at the Γ -point of these two bands with the effective mass of photon in a Fabry-Perot cavity of half-wavelength spacer, made by the same material as our structure $n_C = n_{PC} = 3.15$, for photon having energy levels of $E_1 = 1500$ meV (average photon energy of Band 1), and $E_2 = 1700$ meV (average photon energy of Band 3). In such kind of Fabry-Perot resonator, photon has parabolic dispersion as shown in Ref. [35]. Hence, we got $m_e/m_1^* = 1.08 \times 10^5$ (Band 1), and $m_e/m_3^* = 9.54 \times 10^4$ (Band 3). The photons in both bands are lighter than the corresponding photon in Fabry-Perot cavity, except in Band 3 for structures having FF between 0.47 and 0.48, where there is ultraflat band.

We finish by discussing the extension of the BICs at Γ -point. The extension of the BICs in the Fourier space is characterized by the value k_0 of the wavenumber k_x such that for all wavenumber k_x satisfying $|k_x| < k_0$, $Q > 10^5$. The values of k_0 for both Band 1 and Band 3 in terms of the ratio m_e/m^* are shown in Fig.5(b). Although the data were collected from two different bands with different types of dispersion, they seem to express coherently a function of k_0 in terms of m_e/m^* when combined together, despite a gap from $m_e/m^* = -4 \times 10^5$ to $m_e/m^* = -2 \times 10^5$. Going down from $m_e/m^* = 6 \times 10^5$ (parabolic dispersion of Band 3, positive effective mass) to $m_e/m^* = 0$ (ultraflat band), the value of k_0 significantly rises from $0.028 \mu\text{m}^{-1}$ to $0.403 \mu\text{m}^{-1}$, *i.e.* the BIC extends as the band gets flatter. At $FF = 0.48$, we have an unprecedented situation: (1) ultraflat band with photonic modes of infinite mass, and (2) BIC with large extension causing this ultraflat band to have high Q factor with very long lifetime photon. Especially, the photon at Γ -point has infinite lifetime due to the presence of the Γ -BIC. Such situation is called an extended BIC with infinite mass photon on ultraflat band.

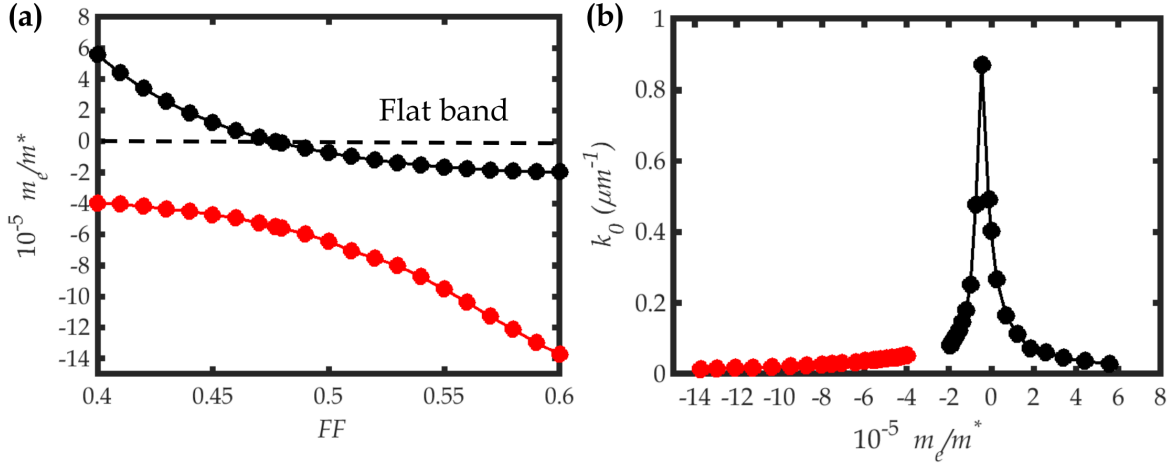


FIG. 5. (a) The effective mass of photon in Band 1 (red) and Band 3 (black). (b) The value k_0 in terms of m_e/m^* , where k_0 is the value of k_x such that for all k_x satisfying $|k_x| < k_0$: $Q > 10^5$. The data were collected from Band 1 (red) and Band 3 (black).

The situation is more complicated in the case of multivalley dispersion. When the photon becomes lighter (the negative ratio m_e/m^* gets larger in absolute value), the quasi-BIC separates from the Γ -BIC, leading to the expansion of the region in Fourier space within which $Q > 10^5$, whereas the Q factor in the region bounded by the two BICs decreases at each value of the wavenumber k_x . That explains why k_0 still becomes higher as m_e/m^* decreases, and we do not have the highest k_0 at flatband, but at $m_e/m^* = -8.71 \times 10^4$, with $k_0 = 0.871 \mu m^{-1}$, corresponding to $FF = 0.49$, when the quasi-BIC starts to separate from the Γ -BIC as previously discussed and shown in Fig.3. In this case, we obtained a multivalley band of high Q factor over a large region of the Fourier space.

By further decreasing m_e/m^* , the Q factor in the region bounded by the Γ -BIC and the quasi-BIC further goes down, leading to a sudden reduction in k_0 . Since then, k_0 only represents the width of the symmetry-protected BIC at Γ -point. The value of k_0 continues to decrease as the effective mass of the photon at Γ -point goes down. That means, the Γ -BIC becomes narrower. Moreover, due to the reduction in the Q factor in the region bounded by the Γ -BIC and the off- Γ quasi-BIC, the portion of dispersion curve of Band 3 between those two points becomes thicker and thick enough to be observed on the reflectivity spectrum as shown in Fig.2. When we further decrease the negative value of m_e/m^* for the parabolic dispersion of Band 1, k_0 decreases. We have the same conclusion for parabolic dispersion with negative curvature as the same kind of dispersion having positive curvature: the symmetry-protected Γ -BIC extends for heavier photon, and reduces in size for lighter photon. Note that the values of k_0 on this band do not

exceed the values of k_0 on Band 3 in case of multivalley dispersion and ultraflat band.

VI. CONCLUSION

In conclusion, by breaking the vertical symmetry to allow the coupling between photonic modes of opposite parities, we have created the coexistence between a symmetry-protected BIC and an off- Γ quasi-BIC on the same band with high Q factor over a broad range of momentum. Furthermore, by parameter-tuning, we also tailored the dispersion characteristics of the photonic modes, changing this band from multivalley to ultraflat band and parabola, and modifying the effective mass of photon in the photonic crystal. By engineering both the real and the imaginary parts of the photonic eigenvalue, we obtained the so-called extended BIC on ultraflat band, with photon having infinite effective mass and very long lifetime. We also proposed an analytical model based on the coupled-mode theory to explain this phenomenon. This work would suggest the way of engineering the photonic eigenvalue on the whole complex plane, promising applications like microlasing, and to study fundamental physical phenomena such as the confinement of photonic modes and the Josephson localization of light.

VII. ACKNOWLEDGEMENT

The authors would like to thank the supports from the project POPEYE for during this research.

-
- [1] J. von Neumann and E. Wigner, *Z.Physics* **30**, 465 (1929).
 - [2] D. R. Herrick, *Physica B* **85**, 44 (1977).
 - [3] F. H. Stillinger, *Physica B* **85**, 270 (1977).
 - [4] H. Friedrich and D. Wintgen, *Physical Review A* **32**, 3231 (1985).
 - [5] C. W. Hsu, B. Zhen, A. D. Stone, J. D. Joannopoulos, and M. Soljačić, *Nature Reviews Materials* **1**, 16048 (2016).
 - [6] M. Robnik, *Journal of Physics A: General Physics* **19**, 3845 (1986).
 - [7] C. M. Linton and P. McIver, *Wave Motion* **45**, 16 (2007).
 - [8] P. J. Cobelli, V. Pagneux, A. Maurel, and P. Petitjeans, *Journal of Fluid Mechanics* **666**, 445 (2011).
 - [9] N. Moiseyev, *Physical Review Letters* **102**, 1 (2009).
 - [10] M. L. de Guevara, F. Claro, and P. A. Orellana, *Physical Review B - Condensed Matter and Materials Physics* **67**, 1 (2003).
 - [11] M. L. Ladrón De Guevara and P. A. Orellana, *Physical Review B - Condensed Matter and Materials Physics* **73**, 1 (2006).
 - [12] F. Capasso, C. Sirtori, J. Faist, D. L. Sivco, S.-N. G. Chu, and A. Y. Cho, *Nature* **358**, 565 (1992).
 - [13] J. U. Nöckel, *Physical Review B* **46**, 15348 (1992).
 - [14] H. Friedrich and D. Wintgen, *Physical Review A* **31**, 3964 (1985).
 - [15] L. S. Cederbaum, R. S. Friedman, V. M. Ryaboy, and N. Moiseyev, *Physical Review Letters* **90**, 4 (2003).
 - [16] R. Thomas, M. Chilcott, E. Tiesinga, A. B. Deb, and N. Kjærgaard, *Nature communications* **9**, 4895 (2018).
 - [17] T.-P. Vo, A. Rahmani, A. Belarouci, C. Seassal, D. Nedeljkovic, and S. Callard, *Optics Express* **18**, 26879 (2010).
 - [18] J. Lee, B. Zhen, S. L. Chua, W. Qiu, J. D. Joannopoulos, M. Soljačić, and O. Shapira, *Physical Review Letters* **109**, 1 (2012).
 - [19] C. W. Hsu, B. Zhen, J. Lee, S. L. Chua, S. G. Johnson, J. D. Joannopoulos, and M. Soljačić, *Nature* **499**, 188 (2013).
 - [20] Y. Yang, C. Peng, Y. Liang, Z. Li, and S. Noda, *Physical Review Letters* **113**, 1 (2014).
 - [21] B. Zhen, C. W. Hsu, L. Lu, A. D. Stone, and M. Soljačić, *Physical Review Letters* **113**, 1 (2014).
 - [22] B. Zhen, C. W. Hsu, Y. Igarashi, L. Lu, I. Kaminer, A. Pick, S.-L. Chua, J. D. Joannopoulos, and M. Soljačić, *Nature* **525**, 354 (2015).
 - [23] A. Kodigala, T. Lepetit, Q. Gu, B. Bahari, Y. Fainman, and B. Kanté, *Nature* **541**, 196 (2017).
 - [24] H. F. Wang, S. K. Gupta, X. Y. Zhu, M. H. Lu, X. P. Liu, and Y. F. Chen, *Physical Review B* **98**, 1 (2018).
 - [25] A. A. Yanik, A. E. Cetin, M. Huang, A. Artar, S. H. Mousavi, A. Khanikaev, J. H. Connor, G. Shvets, and H. Altug, *Proceedings of the National Academy of Sciences* **108**, 11784 (2011).
 - [26] K. Hirose, Y. Liang, Y. Kurosaka, A. Watanabe, T. Sugiyama, and S. Noda, *Nature Photonics* **8**, 406 (2014).
 - [27] A. A. Bogdanov, K. L. Koshelev, P. V. Kapitanova, M. V. Rybin, S. A. Gladyshev, Z. F. Sadrieva, K. B. Samusev, Y. S. Kivshar, and M. F. Limonov, *Advanced Photonics* **1**, 1 (2019).
 - [28] H. S. Nguyen, F. Dubois, T. Deschamps, S. Cuffe, A. Pardon, J. L. Leclercq, C. Seassal, X. Letartre, and P. Viktorovitch, *Physical Review Letters* **120**, 66102 (2018).
 - [29] In preparation.
 - [30] M. G. Moharam, T. K. Gaylord, E. B. Grann, and D. A. Pommet, *Journal of the Optical Society of America A* **12**, 1068 (1995).
 - [31] L. Landau and E. Lifchitz, *Physique Théorique Mécanique: Traduction française*, 5th ed. (Mir Moscou, 1994) p. 129.
 - [32] W. Suh, Z. Wang, and S. Fan, *IEEE Journal of Quantum Electronics* **40**, 1511 (2004).
 - [33] K. Koshelev, G. Favraud, A. Bogdanov, Y. Kivshar, and A. Fratalocchi, *Nanophotonics* , 1 (2019), arXiv:1903.04756.
 - [34] C. Kittel, *Introduction to solid state physics*, 8th ed., edited by S. Johnson, P. McFadden, and M. Batey (John Wiley & Sons, Inc, Hoboken, New Jersey, 2005) p. 680.
 - [35] K. Lagoudakis, *The Physics of Exciton-Polariton Condensates* (EPFL Press, Lausanne, 2013) p. 12.